TB11

19th International Symposium of Ballistics, 7–11 May 2001, Interlaken, Switzerland

# OBLIQUE PLATE PERFORATION BY SLENDER ROD PROJECTILES

**D. J. Gee**

*Institute for Advanced Technology, 3925 W. Braker Lane, Austin, Texas 78759, USA.*

This paper describes a recent effort to examine the perforation of stationary oblique steel plates by hypervelocity tungsten-alloy cylindrical rod projectiles. Specifically, simulations have been performed for *L/D* 10 projectiles against one- and two-plate spaced targets inclined with respect to the projectile velocity vector. The plate thickness-to-rod diameter ratio *t/D* varied slightly as did the plate spacing-to-thickness ratio $t_{gap}/t$. For all simulations, $t/D \in [1.2,1.6]$ and $t_{gap}/t \in [0.7,1]$. Two measures of fidelity are the normalized line-of-sight perforation and the residual velocity. Archival test data are compared with the numerical data on this basis. The results presented reflect pre-impact aerodynamic pitch and yaw in the test data but only pitch angle deviation in the numerical data. The simulation and test data are reasonably well correlated and the data suggest that a favorable angle of attack orientation exists and may be related to the impact geometry. Differences in the perforation efficiency for one- and two-plate targets are noted and erosion mechanisms are explored.

## INTRODUCTION

This paper reports on a recent numerical study on the perforation of stationary, finite thickness, oblique steel plates by slender tungsten-alloy cylindrical rod projectiles. One- and two-plate spaced target configurations were examined in order to investigate their effect on the perforation and erosion process. The pre-impact geometry is indicated in Fig. 1 and was selected to closely replicate a set of tests recently conducted by Bless et al. [1]. In those tests scatter in the data were due in part to the impact yaw which can arise from aerodynamic effects, sabot discard dynamics, or to the projectile's natural modes. In the corresponding simulations only deviations in the aerodynamic pitch angle were investigated. The impact velocities were exclusively in the hypervelocity regime and all of the rod projectiles were of similar fineness ratio (*L/D* 10).

Woodward and Baldwin [2] have studied the oblique perforation of steel targets by small steel core armor piercing projectiles. They varied the plate thickness and impact velocity in an attempt to uncover the influence of the failure mode on oblique perforation and to determine the critical obliquity angle for defeat of the 0.30-*cal*. APM2 projectile. It

was found that the mode of target failure was related to the penetration resistance-hardness relationship. Specifically as the target obliquity increased, the hardness at which adiabatic shear begins to cause a reduction in penetration resistance rises (in steel, from about 350 *HV* to 430 *HV*).

There have been several studies [3–5] of note in the area of normal and oblique perforation of finite thickness plates. Projectiles included steel and aluminum rods (including spin-stabilized rifle rounds) against a variety of plates including aluminum, mild steel, and carbon steel. Impact velocities were generally under 1 *km/s* and the intent of the experimental effort was to determine the velocity drop and orientation of the residual projectile. Obliquity angles up to the point where the projectile ricocheted were studied. Forde *et al.* [5] included *L/D* 10 tungsten-alloy rods in a reverse impact configuration. This study was novel in that the rods were instrumented with manganin piezo-resistive stress gauges in an attempt to study the stress wave propagation through the rod and to investigate the material response. Additionally, this study for thin plates with *t/D* of 0.5 was augmented with hydrocode analysis.

Holmberg *et al.* [6] have conducted an experimental investigation with tungsten-alloy rod projectiles and oblique steel plates at impact velocities of 1.5 and 2.5 *km/s*. Their two-part goals were to determine the applicability of sub-scale experimentation and to investigate the influence of hypervelocity impact. They concluded that sub-scale experimental results were generally applicable and that hypervelocity rods were less affected with respect to post-perforation qualities than were ordnance velocity rods. In a numerical study, Liden et al. [7] found that tungsten projectiles were consumed to a larger extent for higher impact velocities. Penetration and perforation have been described in an empirical manner and for a specific set of experimental conditions by Jeanquartier and Odermatt [8]. There, relationships derived from curve-fitting exercises are presented for the perforation limit and residual length/velocity.

## MODELING

The material elastic-plastic strength models are represented by the Johnson-Cook [9] model. In general the material yield strength *Y* depends on strain and strain-rate hardening and thermal softening terms as indicated by the following relationship:

$$Y = \left[ A + B(\varepsilon^p)^N \right] \left[ 1 + C \ ln \ \dot{\varepsilon}^p \right] \left[ 1 - \theta^m \right], \qquad \dot{\varepsilon}^p \le 10^5 s^{-1} \tag{1}$$

where *A, B, C, N,* and *m* are material constants. The equivalent plastic strain rate $\dot{\varepsilon}^p$ and homologous temperature $\theta$ are defined as follows:

$$\dot{\varepsilon}^p = \sqrt{\frac{2}{3} \dot{e}^p_{ij} \dot{e}^p_{ij}}, \qquad \theta = \frac{T - T_R}{T_M - T_R} \tag{2}$$

where $\dot{\varepsilon}^p_{ij}$ is the plastic deviatoric strain rate tensor and $T_M$ and $T_R$ are the material melt and room temperatures, respectively. Material constants are summarized in Table 1.

Table 1. Johnson-Cook material constants.

| | *A (GPa)* | *B (GPa)* | *C* | *N* | *m* | $T_M$ *( eV)* |
|---|---|---|---|---|---|---|
| Tungsten | 1.35 | 0 | 0.06 | 1 | 1 | 0.1485 |
| Steel | 0.7922 | 0.5095 | 0.014 | 0.26 | 1.03 | 0.1545 |

## EXPERIMENTS

Test data have been drawn from two sources in order to compare with the numerical data. A complete description of the experimental setup may be found in the appropriate references and only a brief summary is given here for sake of completeness. Bless *et al.* [1] conducted fifteen shots of tungsten-alloy projectiles into oblique, one-and two-plate spaced target configurations. Most of the projectiles were L/D 10 rods. Several velocities were considered as well as several different tungsten alloys. These were primarily *W-Ni-Fe* or *Wi-Ni-Co*. The target materials were primarily rolled homogeneous armor (RHA) with $t / D \in [0.7, 2.8]$ (although the bulk were for *t/D* 1.6). Pre-impact and post-perforation *x*-rays were taken in order to measure impact yaw, residual length, velocity, and orientation. A comment on the impact yaw is in order. Since practically all impacts occur with various amounts of unintended aerodynamic pitch and yaw, the experimental data are sometimes represented with a single number – the ballistic yaw angle. This angle is sometimes referred to here, incorrectly, as the impact yaw angle. The magnitude of the ballistic yaw angle has been computed as if the aerodynamic pitch and yaw angles were the cartesian components of a vector quantity. For small angles this approximation is more than adequate. The sign of the resultant was taken from the sign of the pitch component and corresponds with the simulation convention. Although out of place here a comment on the numerical data is also in order. The angular deviation for the simulations was aerodynamic pitch, but is referred to as yaw in the text. It is hoped that no further confusion will result from the use of this terminal ballistic convention.

The experimental program of Holmberg *et al.* [6] was conducted with a two-stage light gas gun. Pre-impact and post-perforation *x*-rays were taken to record the condition of the rod. However no ballistic yaw data was included in the report. The L/D 15 projectiles were of a high strength, sintered tungsten-alloy and the plates were armor steel having a Vickers hardness of 300. Two velocities (1.5, 2.5 *km/s*) were chosen and two target obliquity angles (60°, 80°) were selected. The *t/D* ratio varied between 0.4–1.8 in a manner such that the line-of-sight plate thickness was controlled.

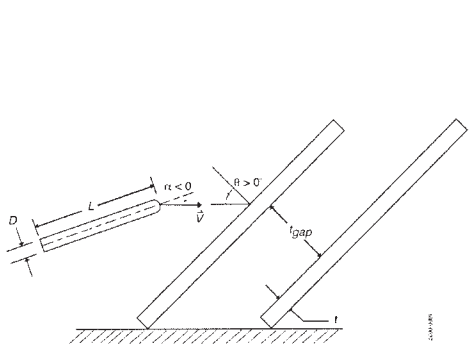


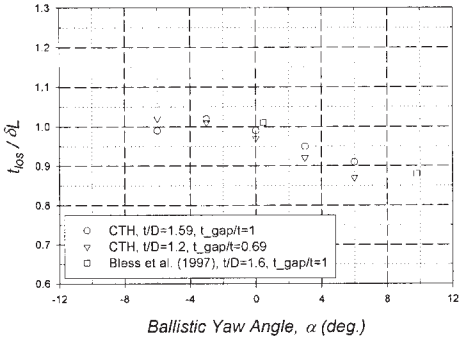


Figure 1. (left) Schematic of pre-impact geometry (not to scale). Pitch angle is indicated (this is consistent with aerodynamic convention where yaw occurs in the orthogonal plane).

Figure 2. (right) Line-of-sight perforation normalized by eroded rod length; $V$=2.6 *km/s* (nom.), $L/D$ 10 tungsten-alloy projectile, 2-plate, spaced steel target, $\theta$=65°.

## RESULTS

Simulations representing the nominal test conditions [1] have been performed for the impact, at 2.6 *km/s*, of one- and two-plate spaced targets including up to ±6° of aerodynamic pitch. For all cases here a residual projectile emerges behind the target. The line-of-sight perforation normalized by the eroded rod length is presented in Fig. 2 as a function of the ballistic yaw angle. Larger values of the ordinate are favorable since they indicate lesser amounts of rod erosion, all other things being equal. The results indicate that for $\alpha = 0°$, erosion and line-of-sight perforation are roughly in balance, even including up to –6° of impact yaw (i.e., pitch away from the plate exterior normal). However, the perforation efficiency does appear to be degraded when the impact yaw is positive. As may be seen the correlation between the numerical and test data (circle and square symbols in Fig. 2) is excellent where test data exists.

Additional simulations were performed to evaluate the effect of decreased gap spacing (triangular symbols in Fig. 2). Clearly, for the smaller gap selected here there is no effective difference in the perforation efficiency. It should be mentioned that in [1] if the residual rod is broken the reported length is the sum of all major segments at least a full diameter D wide. The stated uncertainty in length measurements was ± 0.25 $D$ and since the residual projectile often is broken, the error in the residual length measurement may be larger than the stated uncertainty. It is worth noting that there is close agreement in the residual velocities for the two data sets. For the two-plate data analyzed here, $V_R/V \in$ [0.84, 0.93].

A trend identified by the computations suggests that the nose-up configuration (with respect to the velocity vector) is slightly favorable for minimizing erosion. This is counter to the results of Anderson *et al.* [10] who found that the nose-down impact configuration was favorable for similar materials. Lower perforation times were identified as the signi-

ficant factor in the impact of *L/D* 20 and 36 rod projectiles into finite thickness targets with *t/D* 1.9. Material plots for the two extreme cases ($\alpha = \pm 6°$) illustrates the phenomenology of the perforation process. For $\alpha = -6°$ (Fig. 3a–e), the material plots show that early time interaction includes the formation of a slot cut into the front face of the first plate, Fig. 3a. This tends to impart a clockwise pitching moment to the rod (once the lateral interface moves behind the rod center-of-gravity) and also gives rise to a vertical velocity component. For later times (Figs. 3b–c), rod rotation tends to re-align the rod axis along the original trajectory. Upon exit from the second plate and noting the slight upward change in elevation (Fig. 3d), it can be shown that the late-time path through the target is very similar to the $\alpha = 0°$ case. For $\alpha = +6°$ (Fig. 3f–j), the case is little, but noticeably, different. Slot formation occurs much later with a slot being cut into the rear face of the front plate, Fig. 3g. The late-time interaction is insufficient to completely re-align the rod along the original trajectory. Also it can be seen that the counter-clockwise induced pitching moment tends to pitch the rod into the plate and therefore away from the bulged region, Fig. 3h. Upon exit (Fig. 3i), the residual rod is noticeably yawed. For this case the pitching moment due to slot interaction and asymmetric exit conditions are of opposite sense whereas in the case for $\alpha = -6°$ the pitching moments are of the same sense. It should be mentioned that the effect of + 6° nose-down yaw on perforation efficiency is small and amounts to roughly 0.5 *D* of increased erosion. Finally it may appear from this sequence of material plots (specifically, Figs. 3c and 3h) that there is a small difference in elapsed perforation time for the two extremum cases. However, the nominal interaction dynamics for the two cases are different due to angle of attack and target obliquity issues and therefore a comparison based simply on equivalent simulation time is not appropriate. For the relatively thin plates considered here, the path angles through the target are similar.

In addition to angle-of-attack considerations it is also of interest to investigate the effect of impact velocity and of multiple, spaced-plates on erosion. Computations have been performed for *L/D* 10 projectiles impacting a one-plate target at 2.1 and 2.6 *km/s* and one- and two-plate spaced steel targets at 2.6 *km/s*. This data along with data from [1], [6] are shown in Fig. 4. The test data [1] are for slightly larger *t/D* and $t_{gap}/t$ ratio. The target obliquity angle, however, corresponds to that numerically simulated. Also the single-plate data of Holmberg *et al.* [6] are for different *t/D* values, *L/D* values, obliquity angles, and impact velocities. Overall the numerical and test data are reasonably well correlated even though no corrections have been applied to the data to account for the mismatch in impact conditions or materials.

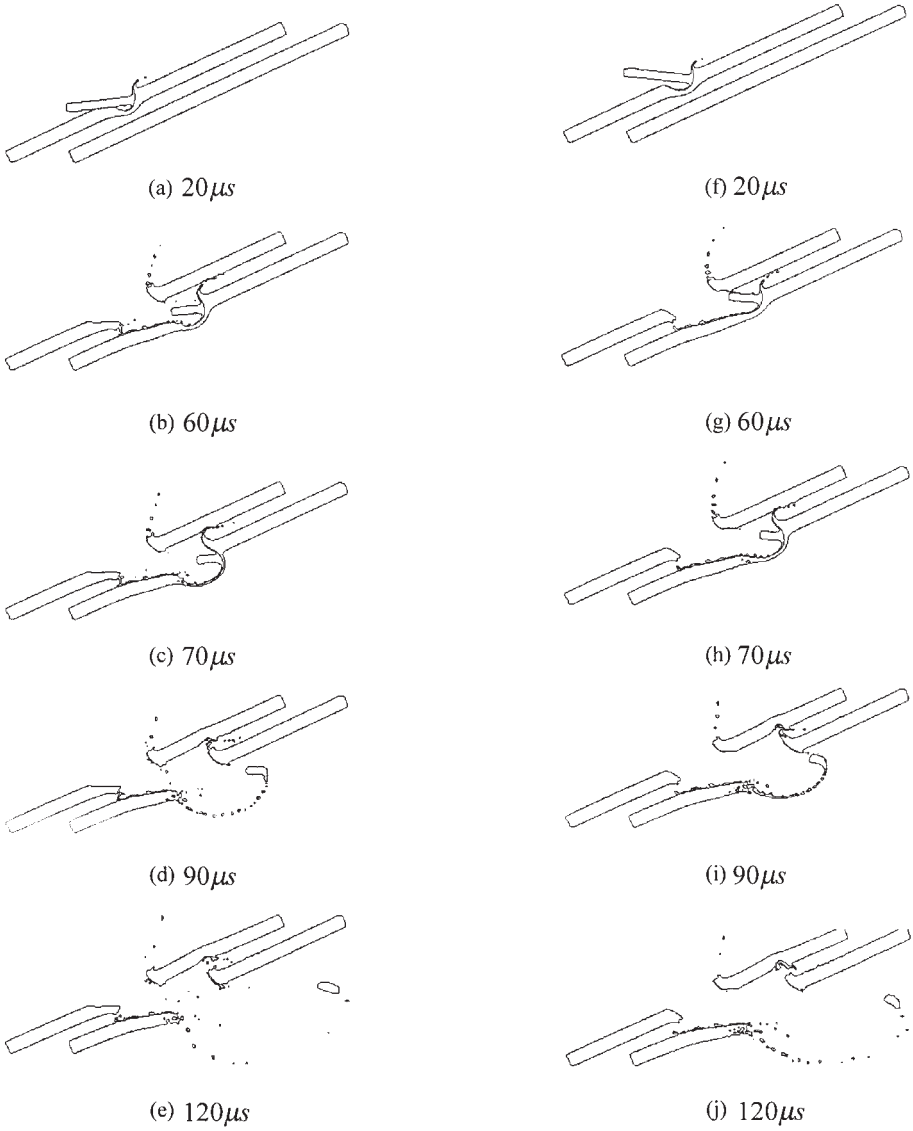


Figure 3. Material plots for the impact of a tungsten-alloy projectile into a 2-plate, spaced steel target at 2.6 km/s: (a–e) $\alpha = -6°$, (f–j) $\alpha = +6°$.

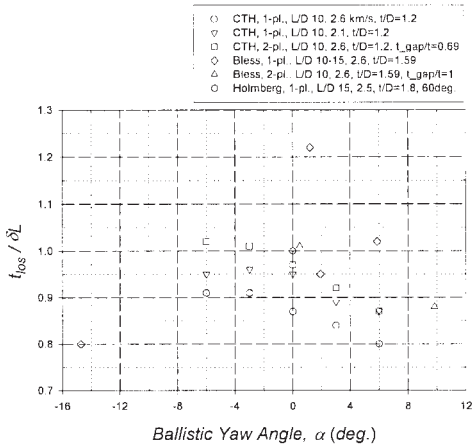


Figure 4. Line-of-sight perforation normalized by eroded rod length. 1- and 2-plate spaced steel targets with $\theta = 65°$ (unless otherwise noted); *L/D* 10, 15 tungsten-alloy projectiles.

The data suggests that the normalized line-of-sight perforation is only mildly sensitive to impact velocity (at least for the velocities considered here) as the differences in erosion amount to approximately 0.25 *D* or less for the two impact velocities (circle and inverted triangular symbols in Fig. 4). The data also suggests a synergistic effect with respect to rod erosion in having the second plate close behind the first. This is demonstrated by the higher perforation efficiencies across the yaw range when comparing the one- and two-plate calculations (circle and square symbols in Fig. 4). The difference in perforation efficiency for $\alpha = 0°$ corresponds to roughly 0.7 *D* less erosion in the multi-plate case. That is, for a simple scaling the predicted erosion for two single-plate targets spaced far enough apart would be 0.7 *D* more than found in the two-plate, spaced target modeled here. There are at least two possible explanations, measurement uncertainty notwithstanding. One may be that behind-armor-debris from the first plate precedes the rod into the second plate (Fig. 5a). In this way perforation is initiated by debris rather than projectile. A second plausible explanation may be related to the gap length between the plates. Since the rod will continue to erode in the gap due to unequilibrated penetration and tail velocities, maximal erosion will not be attained if the gap length is insufficient to take advantage of the transient residual stress state induced in the rod as a result of impact with the first plate.

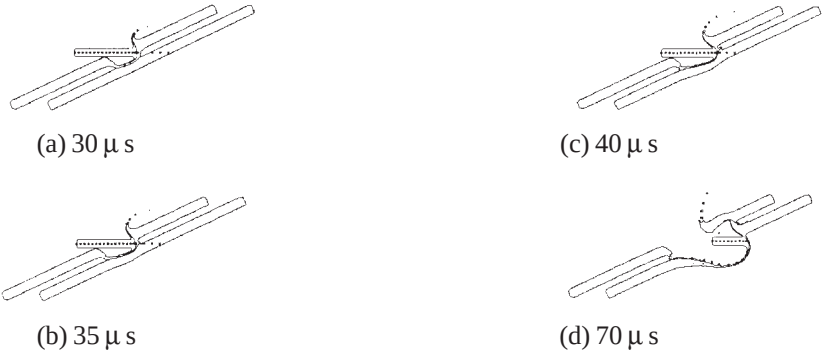


Figure 5. Material plots for the impact of a tungsten-alloy projectile into a 2-plate, spaced steel target at 2.6 *km/s* and $\alpha = 0°$; $t/D = 1.2$, $t_{gap}/t = 0.69$.

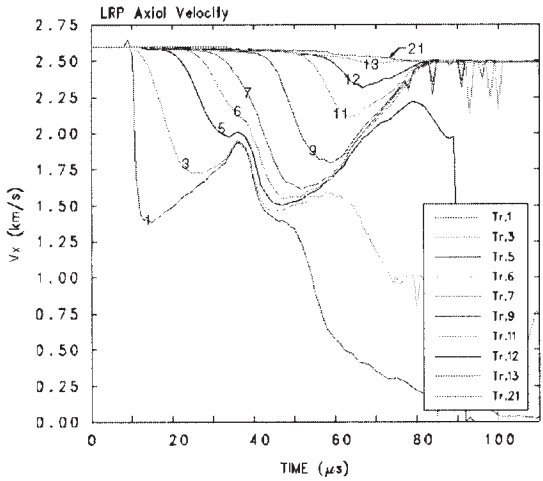


Figure 6. Axial velocity data for select positions along projectile; 2-plate, spaced steel target at 2.6 *km/s* and $\alpha = 0°$; $t/D = 1.2$, $t_{gap}/t = 0.69$.

To explore this idea further we have examined plots of the projectile's axial velocity for select locations. The axial velocity component can be used to approximate the penetration velocity if the projectile's lateral velocity component (here, due to oblique impact) is much smaller than the former. This condition is satisfied here. Select axial velocity data for the two-plate array are displayed in Fig. 6. It is not clear from this plot when the projectile breaks out from plate #1 and moves in the space between the plates. In fact it can be seen in Figs. 5a–c that any calculation for between-plate erosion will not be objective. It is clear though that the penetration and tail velocities have not fully equilibrated before the rod initiates impact with the next plate. It was estimated that for t between 35–37 μs the rod tip may be considered to be between plates. The between-plate erosion may be computed by integrating the relation

$$\dot{L} = (u - v) \tag{3}$$

where $u$ is the penetration velocity and $v$ is the tail velocity. The simple result

$$\delta L = (\tilde{u} - v)\delta t \tag{4}$$

is obtained if $u(t)$ is assumed to vary linearly over the time interval of interest. Hence $\tilde{u}$ in this formulation is the average penetration velocity over the relevant time interval. In this way the between-plate erosion was estimated to be 0.12 $D$.

Next a similar process is used to calculate the behind-plate erosion. Breakout from the rear plate (plate #2) is indicated in Fig. 5d. It can be shown that the interface pressure has essentially dropped to zero for this time. In Fig. 6 it can be seen that the residual penetration velocity is approximately 2.3 *km/s* and fully equilibrates with the tail velocity after approximately 12 $\mu s$. During this interval the behind-plate erosion was estimated from Eq. (4) to be 0.13 $D$. This estimate is consistent with that found for behind-plate erosion in the one-plate ($t/D$ 1.2) target for $V_o$ = 2.6 *km/s*. Thus it seems apparent that the lack of full equilibration for $u$ and $v$ between plates does not adequately address the differences in perforation efficiencies for the one- and two-plate targets. Some other as yet undetermined mechanism would seem to be the cause. Finally we note that the line-of-sight perforation efficiency for the one- and two-plate data of [1] show no such synergism as the single-plate data are somewhat scattered. It is difficult to characterize the data of Holmberg *et al.* [6] since the impact yaw, if non-negligible, was not stated. We have simply plotted it here as if it were for $\alpha = 0°$.

## CONCLUSIONS

Simulations have been performed for the through-penetration of oblique steel plates by $L/D$ 10 tungsten-alloy rod projectiles. Primary simulation parameters have included impact yaw angle, number of plates, and impact velocity. Additionally some variations in plate thickness-to-rod diameter ratio and plate gap spacing have been included as well. It has been shown that the normalized line-of-sight perforation efficiency is only mildly sensitive to impact velocity (at least for the two considered here). Furthermore it appears that rod erosion for the closely spaced, multi-plate target is not simply a scalar multiple of the single-plate case. Some synergism with respect to erosion in having the second plate close behind the first was evident but it was demonstrated that this was not due to issues related to between-plate erosion. It has also been shown that the perforation efficiency is sensitive to small amounts of impact yaw. For late-times the nose-up case appears indistinguishable from the $\alpha = 0°$ case due to early slot formation and asymmetric exit conditions. In these cases the perforation efficiencies are similar. The nose-down case includes pitching moments that are of opposite sense. These cases are more easily distinguishable from the $\alpha = 0°$ case and also show some degradation in the perforation efficiency. The numerical data generally compare favorably with archival test data conducted under similar conditions.

**Acknowledgment** – The author wishes to thank Dr. Sikhanda Satapathy for valuable discussions on this work. This work was supported by the U.S. Army Research Laboratory (ARL) under contract DAAA21-93-C-0101.

## REFERENCES

1. Bless, S.J. *et al.*, "Penetration of oblique plates," IAT.R 0149, Institute for Advanced Technology, University of Texas at Austin, 1–25, 1997.
2. Woodward, R.L. and Baldwin, N.J., "Oblique perforation of targets by small armor-piercing projectiles," *J. Mech. Eng Sci. 21*, 85–91, 1979.
3. Goldsmith, W. and Finnegan, S.A., "Normal and oblique impact of cylindro-conical and cylindrical projectiles on metallic plates," *Int. J. Impact Eng.* 4(2), 83–105, 1986.
4. Gupta, N.K. and Madhu, V., "Normal and oblique impact of a kinetic energy projectile on meld steel plates," *Int. J. Impact Eng.* 12(3), 333–343, 1992.
5. Forde, L.C. et al., "Experimental investigation and analysis of penetration in oblique impact," *Proc. 16th Int. Bal. Sym.*, San Francisco, CA, 641–649, Sept. 1996.
6. Holmberg, L., Lundberg, P., and Westerling. L., "An experimental investigation of WHA long rods penetrating oblique steel plates," *Proc. 14th Int. Bal. Sym.*, Quebec, Canada, 515–524, Sept. 1993.
7. Liden, E., Ottosson, J., and Holmberg, L. "WHA long rods penetrating stationary and moving oblique steel plates," *Proc. 16th Int. Bal. Sym.*, San Francisco, CA, 703–711, Sept. 1996.
8. Jeanquartier, R. and Odermatt, W., "Post-perforation length and velocity of KE projectiles with single oblique targets," *Proc. 15th Int. Bal. Sym.*, Jerusalem, lsrael, 245–252, May 1995.
9. Johnson, G.R. and Cook, W.H., "A constitutive model and data for metals subjected to large strains, high strain rates and high temperatures," *Proc. 7th Int. Bal. Sym.*, Hague, Netherlands, 541–547, 1983.
10. Anderson Jr., C.E. et al., "Investigation of yawed impact into a finite target," Proc. Am. Phys. Soc. Topical Group on Shock Compression of Condensed Matter, MA, July 1997.